Electrochemically Exfoliating MoS$_2$ into Atomically Thin Planar-Stacking Through a Selective Lateral Reaction Pathway

Xuelei Pan, Mengyu Yan, Congli Sun, Kangning Zhao, Wen Luo,* Xufeng Hong, Yunlong Zhao, Lin Xu, and Liqiang Mai*

The production of atomically thin transition-metal dichalcogenides (TMDs) has been investigated through various top-to-down exfoliation methods, such as mechanical and chemical exfoliation, while large-scale chemical exfoliation is sluggish and needs over ten hours to achieve atomically thin TMDs. Herein, a new strategy is reported for exfoliating bulk MoS$_2$ into two/three-layer flakes within tens of seconds through a mild electrochemical treatment. This exfoliation method is driven by a lateral inward oxidation reaction starting from the typical layer edge with a rapid depth penetration, whereby a stacked few-layer (two/three layers) structure is ultimately formed. This efficient reaction process is monitored based on an individual MoS$_2$ on-chip device combined with in situ Raman and cross-sectional scanning transmission electron microscopy, and the uniformity of thickness is demonstrated. This preferentially initiated method can be also extended to produce few-layer MoSe$_2$ and the selective extraction mechanism is assumed to be related to intrinsic layer-dependent energy band properties. Moreover, the special reassembled few-layer MoS$_2$ possesses great performance as functional materials in electrocatalysis (127 mV overpotential for hydrogen evolution reaction) and surface-enhanced Raman spectroscopy (10^5 enhancement factor). These results illustrate the broad prospects of the reassembled few-layer MoS$_2$ for optics, catalysis, and sensors.

1. Introduction

Transition-metal dichalcogenides (TMDs) are typical 2D materials with fantastic and tunable physicochemical properties.[1,2] Atomically thin TMDs attract broad attention and have been explored in widespread fields, such as electronics/optical devices,[3,4] sensors,[5] catalysis,[6–8] and energy storage,[9,10] etc. The atomic thickness of 2D TMDs endows the quantum confinement in the electronic structure, which holds great promise for the aforementioned fields and leads to the research on producing monolayer or few-layer TMDs.[11,12] Up to now, researches on the production of atomically thin TMDs focus on two fields, "top-to-down" exfoliation methods[13–15] and "bottom-to-up" chemical vapor growth.[16–18] The former method uses the shear force to break the interlayer van der Waals (vdW) interaction by mechanical methods or ion/molecule intercalation, and the latter is based on chemical vapor deposition. Although

X. Pan, Prof. C. Sun, Dr. W. Luo, X. Hong, Prof. L. Xu, Prof. L. Mai
State Key Laboratory of Advanced Technology for Materials Synthesis and Processing
International School of Materials Science and Engineering
Wuhan University of Technology
Wuhan 430070, P. R. China
E-mail: luowen_1991@whut.edu.cn; mlq518@whut.edu.cn
Dr. M. Yan
Department of Materials Science and Engineering
University of Washington
Seattle, WA 98105, USA
Prof. C. Sun
Nanostructure Research Centre (NRC)
Wuhan University of Technology
Wuhan 430070, P. R. China

Dr. K. Zhao
Laboratory of Advanced Separations (LAS)
École Polytechnique Fédérale de Lausanne (EPFL)
Sion CH-1951, Switzerland
Dr. W. Luo
Department of Physics
School of Science
Wuhan University of Technology
Wuhan 430070, P. R. China
Prof. Y. Zhao
Advanced Technology Institute
University of Surrey
Guildford, Surrey GU2 7XH, UK
Prof. Y. Zhao
National Physical Laboratory
Teddington, Middlesex TW110LW, UK
Prof. L. Mai
Foshan Xianhu Laboratory of the Advanced Energy Science and Technology Guangdong Laboratory
Xianhu Hydrogen Valley
Foshan 528200, P. R. China

ADVANCED
SCIENCE NEWS
www.advancedsciencenews.com

ADVANCED
FUNCTIONAL
MATERIALS
www.afm-journal.de

the exfoliation methods can achieve high-quality 2D crystals, the scalable exfoliation is challenging and takes a long time.[19] Chemical vapor synthesis can achieve large-scale 2D TMDs with controlled thickness,[20,21] while it requires high temperature and precise conditions and also introduces abundant crystallographic defects.[22,23] In general, the rapid and mild approach to achieve atomically thin TMDs remains an important issue. In addition to TMDs, tremendous 2D materials have been developed, such as MXenes,[24] silicene,[25] and hexagonal boron nitrides,[26] etc. Different from the exfoliation of TMDs, MXene is a typical 2D material obtained by selective removing the "A" atom layer from bulk MAX material.[27] Thus, MXene can be produced on a large scale and its application in energy storage and conversion is realized.[28,29] Recently, researchers have reported the transformation of non-vdW bulk crystals to 2D TMDs by reaction with chalcogen vapor.[30] This is a novel approach that imitates the exfoliation method of MXene, which utilizes a chemical reaction to extract certain atom layers to reduce bulk crystal into 2D TMDs. Nevertheless, this method must be operated at a high temperature, and the obtained accordion-like TMD is limited by the size and uniformity. Besides, researchers have reported a photo-induced exfoliation method[31] that realized the transformation from bulk to monolayer TMDs, unfortunately it discards most of bulk materials. In addition to the difficulty in the efficient exfoliation approach, the exploration of the exfoliation mechanism is another crucial problem. In the above work of photo-induced exfoliation, the optical observation contributes to the understanding of the exfoliation process. Nevertheless, the investigation of traditional exfoliation is limited by the lack of dynamic observation, and the inheritance of exfoliated sheets cannot be achieved. A systematic research model based on the individual TMD sheet is urgent for the development of 2D materials.

In light of the previous work, a mild method for achieving atomically thin 2D TMDs in high-efficiency and high-yield is eager. Herein, we demonstrate an electrochemical strategy to realize the fast transformation from bulk to 2D TMDs. Based on the on-chip device, we focused on the individual MoS_2 sheet and found that when a high anodic potential is applied to bulk MoS_2 in sulfate electrolyte, the edge of bulk MoS_2 is selectively etched and the reaction subsequently proceeds to create a 2D channel. As shown in **Figure 1**, the uniform bi/tri-layer MoS_2 layers were finally retained and formed a stacked structure.

This phenomenon is attributed to the oxidation of MoS_2 to a high valance state leading to a selective structure degradation in the 2D channel. This electrochemical exfoliation method is an efficient strategy that directly transforms high-quality bulk to atomically thin 2D TMDs. It produces atomically thin MoS_2 in a short time and the formed uniform stacked few-layer 2D TMDs show considerable application potential. The exfoliated few-layer MoS_2 shows a relatively low overpotential (127 mV at 10 mA cm^{-2}) for hydrogen evolution reaction. Moreover, it also shows high surface-enhanced Raman spectroscopy (SERS) sensitivity for R6G molecule (target analyte), the lowest detectable concentration is 10^{-8} M and the enhancement factor is more than 10^5.

2. Results and Discussion

To focus on the dynamic structure evolution of an individual TMD sheet, we fabricated an on-chip electrochemical device based on an individual MoS_2 sheet. Herein, the sheets with a thickness of more than tens of nanometer are denoted as bulk MoS_2. One layer of poly(methyl methacrylate) (PMMA) was used as the covering layer to insulate gold electrodes. A window was opened by e-beam lithography (EBL) to expose the specific region of MoS_2 sheet to the electrolyte. According to the conventional ion-intercalation exfoliation cases, the intercalated ions expand the interlayer space of MoS_2, and the following chemical and mechanical treatment break the vdW interaction between layers.[15] Particularly, MoS_2 has been demonstrated to be able to store zinc ions after expanding the interlayer space. In this regard, we firstly applied a similar exfoliation treatment on the MoS_2 sheet in an aqueous solution (1 M zinc sulfate solution).[32,33] We performed the cyclic voltammetry (CV) test of the individual MoS_2 sheet in the region corresponding to the zinc ion intercalation potential (Figure S1a, Supporting Information). However, the weak electrochemical signal suggested that the intercalation of zinc ion into the interlayer of pristine MoS_2 is quite difficult. This can be attributed to the larger radius of hydrated zinc ion (≈5.1 Å) than the interlayer space (≈3.1 Å) of MoS_2. Nevertheless, we found that when the CV test was performed in a higher potential region (0.2–1.4 V vs SCE), an obvious redox transition was captured (Figure S1b, Supporting Information). And the first several CV cycles show
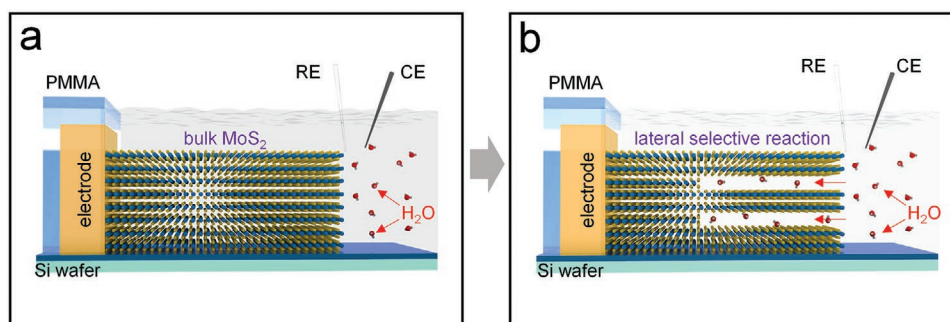

Figure 1. The schematic illustration of selective exfoliation of bulk MoS_2 and the formed stacked structure. a) The schematic of the on-chip device based electrochemical configuration. RE and CE represent the reference electrode (saturated calomel electrode, SCE) and counter electrode (Pt electrode). b) The schematic of the process driven by a lateral inward electrochemical reaction and water molecules go into bulk phase through the formed 2D channel.
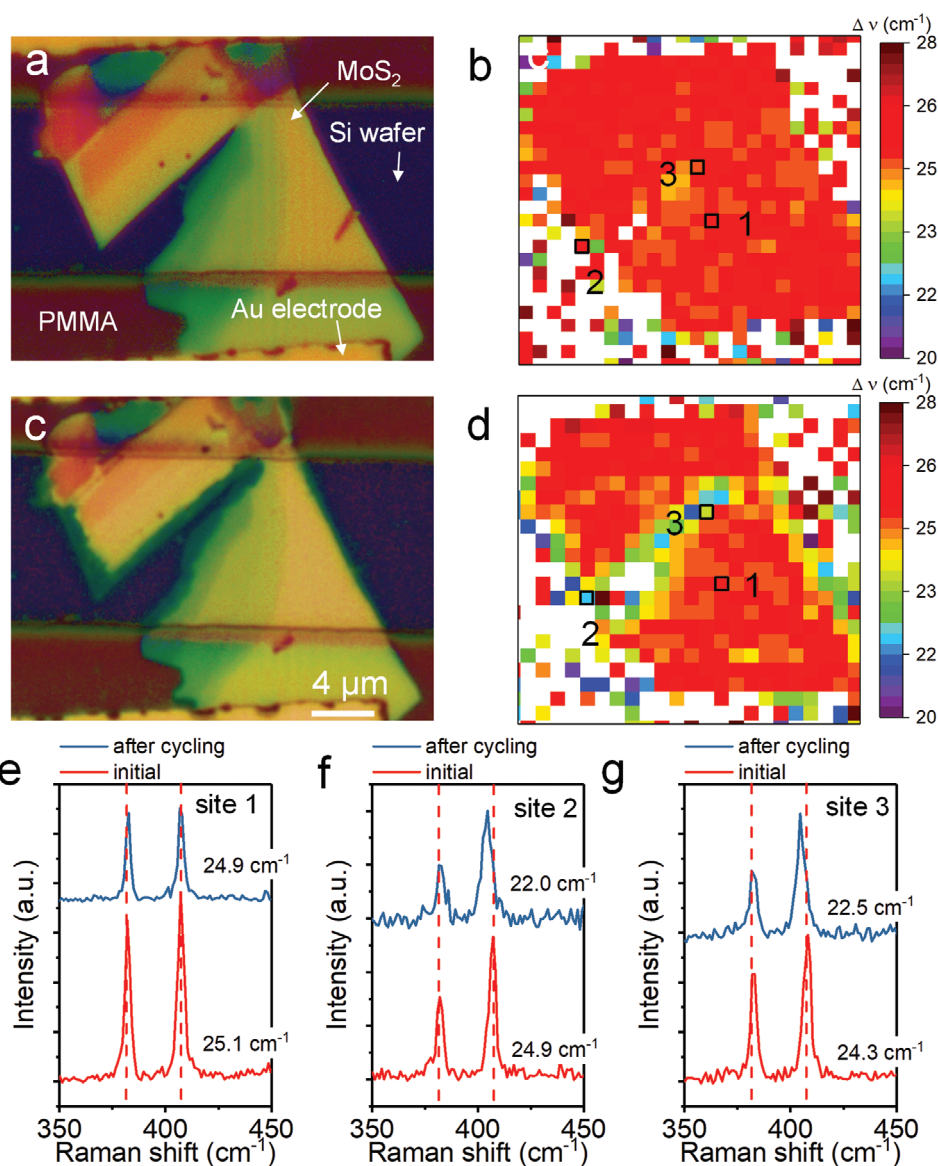
Figure 2. a) Optical image of the individual bulk MoS_2 sheet on a SiO_2/Si wafer (300 nm oxide layer). b) The mapping of the wavenumber difference ($\Delta\nu$) of two typical vibration bands of MoS_2 (E^1_{2g} at ≈383 cm^{-1} and A_{1g} at ≈408 cm^{-1}). c,d) Optical image and mapping of $\Delta\nu$ of the same MoS_2 after electrochemical treatment in the electrolyte of $ZnSO_4$. e–g) Raman spectra of initial MoS_2 and after the treatment at three selected sites.

enhanced oxidation peaks. After achieving this electrochemical signal, we compared the optical image of MoS_2 before and after the CV test (**Figure 2**a,c). It can be found that the MoS_2 edge after the CV test shows a color change from yellow to green (Figure 2c). Technically, color is a simple index for estimating the thickness, and the semitransparent green color empirically implies a thickness of less than 10 nm. To further identify the structure evolution, Raman spectroscopy is used to recognize the characteristic vibration bands. In 2H-phase MoS_2, Mo and S atoms are coordinated in [MoS_6] octahedral, forming an S-Mo-S layer.[34] According to Raman selection rules, there are four first-order Raman-active modes for 2H MoS_2, denoted as E_{1g}, E^1_{2g}, E^2_{2g}, and A^1_g.[35] Specifically, E^1_{2g} and A_{1g} bands can be easily detected around 400 cm^{-1} to reveal the layer-related information. E^1_{2g} (≈383 cm^{-1}) and A_{1g} (≈408 cm^{-1}) bands arise from in-plane

opposite Mo-S vibration and out-of-plane vibration of S atoms (Figure S2, Supporting Information), respectively.[36] Therefore, the thickness of MoS_2 (less than 5 layers) can be determined by calculating the wavenumber difference ($\Delta\nu$) between E^1_{2g} and A_{1g} bands.[35–37] We recorded Raman spectra of the MoS_2 before and after electrochemical treatment and calculated the $\Delta\nu$ of each site (Figure 2b,d). The corresponding wavenumber mapping of E^1_{2g} and A_{1g} bands are shown in Figure S3 in the Supporting Information. Figure 2b shows the distribution of $\Delta\nu$ for the initial MoS_2, which shows uniform $\Delta\nu$ at ≈25 cm^{-1}. For the MoS_2 after electrochemical treatment, corresponding to the color-changed regions, $\Delta\nu$ decreased to ≈22.5 cm^{-1} (Figure 2d). The Raman spectra of selected sites are shown in Figure 2e–g. It has been studied that $\Delta\nu$ decreases to ≈23 and ≈22 cm^{-1} for trilayer and bilayer MoS_2, respectively.[36] Hence, it can be

**ADVANCED
SCIENCE NEWS**
www.advancedsciencenews.com

**ADVANCED
FUNCTIONAL
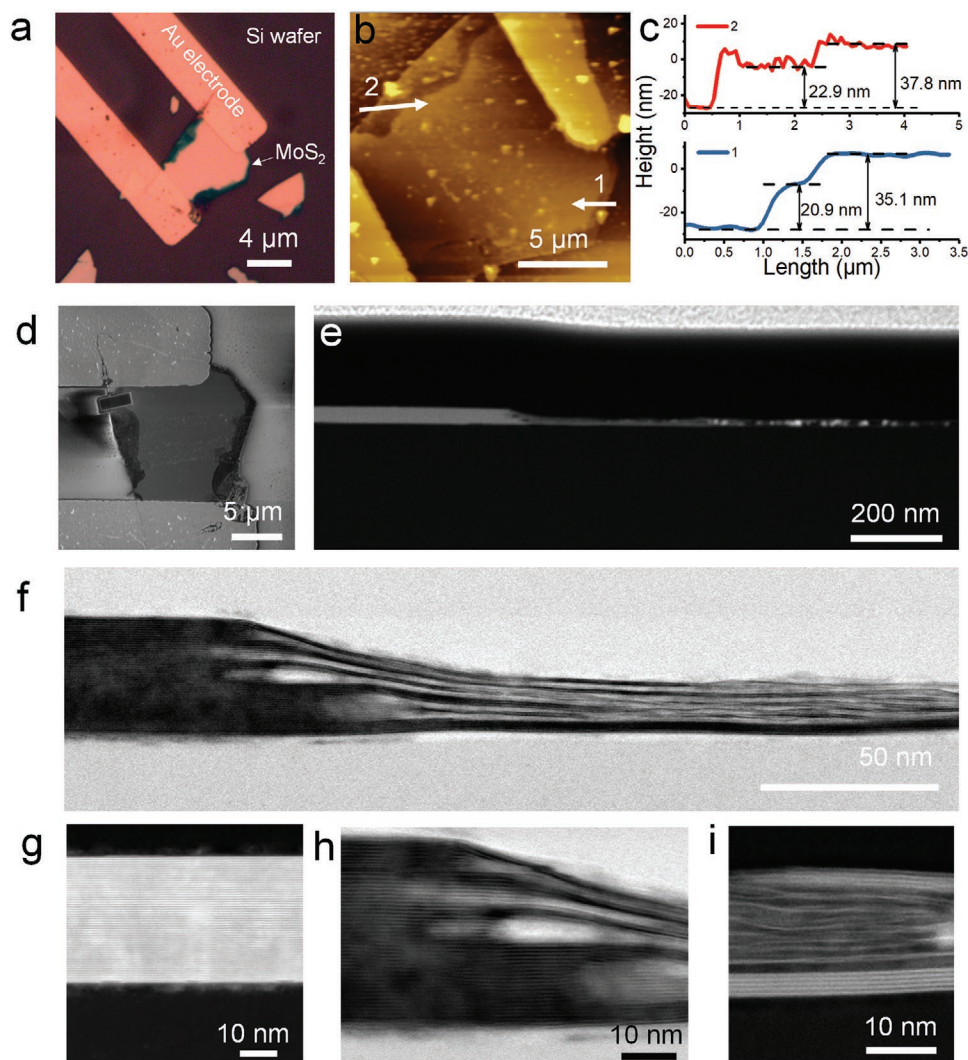MATERIALS**
www.afm-journal.de

Figure 3. a) Optical image of a typical MoS$_2$ sheet after electrochemical treatment (remove PMMA layer). b,c) The corresponding AFM image and the thickness profile along the arrow direction of two lines. d) The SEM image of the same MoS$_2$ sheet with a C/Pt cover layer prepared for FIB. e) An overview of the cross-profile STEM image of the MoS$_2$ sheet. The sample is prepared from the rectangle region in (d). f) The magnified image of the transition zone from bulk to edge. g–i) The magnified STEM images of bulk, transition zone, and edge, respectively.

concluded that the thickness of the MoS$_2$ edge is reduced to trilayer or bilayer after the electrochemical treatment in the ZnSO$_4$ aqueous solution. Few-layer MoS$_2$ is achieved after several CV cycles treatment, and this transformation seems to start from the edge but not exfoliate from the whole surface layer.

To solidly confirm the thickness change and further investigate the structure information, we performed atomic force microscopy (AFM) and scanning transmission electron microscopy (STEM) characterization. **Figure 3a** shows an optical image of individual MoS$_2$ after electrochemical treatment where the green regions are supposed to be involved in the electrochemical reaction. The corresponding AFM image shows a reduced thickness of the MoS$_2$ edge (Figure 3b). The thickness of the MoS$_2$ basal plane is ≈35 nm, while the edge region is reduced to ≈20 nm (Figure 3c). This result seems to contradict the Raman spectra in Figure 2, which shows a mere bilayer/trilayer distribution at the edge region. To identify the structural details of the MoS$_2$ involved in the reaction, we used

the focused ion beam (FIB) to fabricate the cross-sectional sample from the rectangle region in Figure 3d. Figure 3e shows an overview of the cross profile from bulk to the edge. We can find an obvious slope thickness-shrinkage on the transition zone, where the thickness decreased from ≈35 to ≈20 nm. The magnified images of bulk, transition zone, and edge are shown in Figure 3g–i. Some specific layers in MoS$_2$ are extracted from the bulk region and the remained MoS$_2$ layers (most are two/three layers) form a restacked structure with a decreased thickness. It is worth noting that the bottom remains 3–5 layer according to the STEM results. This phenomenon can be attributed to that the strong Coulomb interaction between bottom MoS$_2$ and substrate inhibits the electrochemical reaction.[12,31] To sum and note, this structure has two characteristics: First, the stacked structure with two/three layers is expanded and forms a loose but stable stacking; Second, the stable bottom and top layers of the MoS$_2$ sheet account for the whole outline of MoS$_2$ after electrochemical treatment. These two points
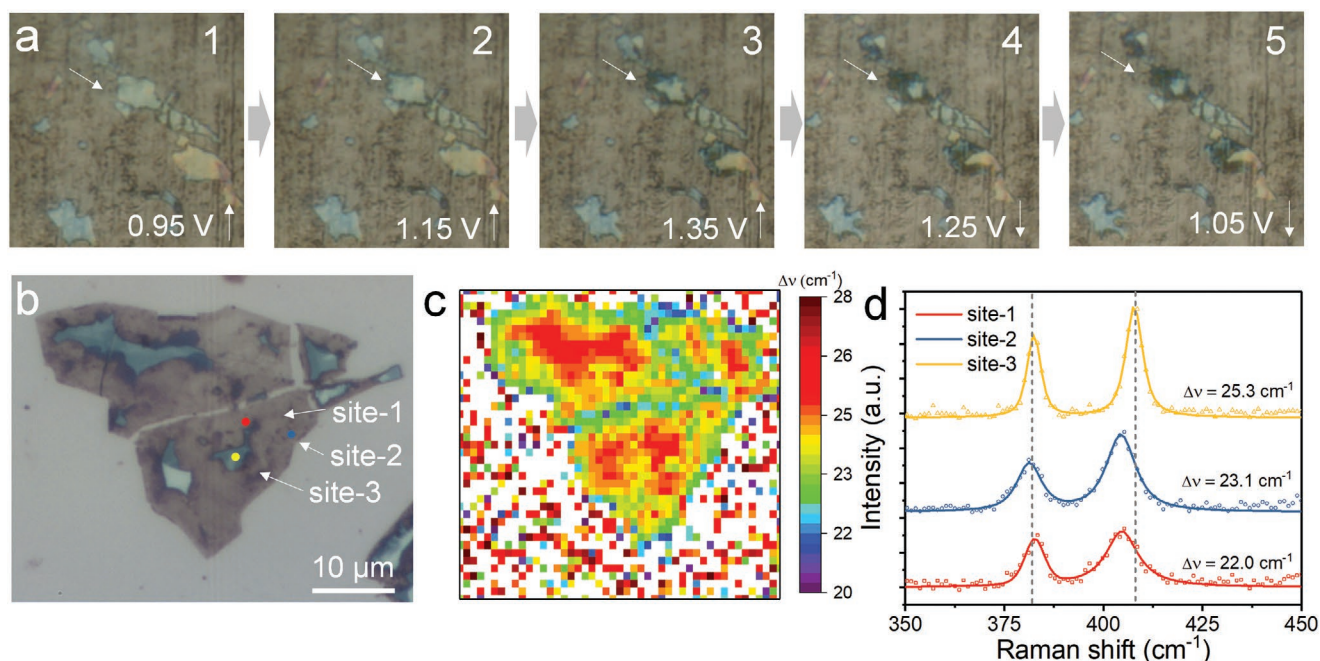
**ADVANCED
SCIENCE NEWS**
www.advancedsciencenews.com

**ADVANCED
FUNCTIONAL
MATERIALS**
www.afm-journal.de

Figure 4. a) The in situ optical snapshots of MoS_2 sheets during an electrochemical process in $ZnSO_4$ electrolyte (first increase to 1.4 V vs SCE and then back). b) Optical image of a typical MoS_2 sheet after the electrochemical treatment on the Ti foil. c) The corresponding mapping of Δv. d) Raman spectra of three selected sites on the MoS_2 sheet in (b).

distinguish this electrochemical exfoliation from conventional corrosion or etching approaches. In conclusion, we can fully understand the results from Raman, AFM, and STEM, that the electrochemical treatment only extracts selective few layers in the bulk MoS_2, and the left uniform two/three-layer reassembles to form a stacked structure and keeps the whole outline of initial MoS_2 sheet intact.

After identifying the structural details of the exfoliated MoS_2 after electrochemical treatment, we further studied the reaction pathway. Based on the aforementioned results, it is rational to hypothesize that this reaction follows an inward propagation pathway, namely begins at the unpacking of edge and then goes straight into the depth. To verify this hypothesis, we fabricated two types of on-chip MoS_2 devices, one exposes the basal plane and another one exposes the edge regions (Figure S4, Supporting Information). After the same electrochemical treatment (CV test in $ZnSO_4$ solution), the plane-exposed MoS_2 shows a stable structure without any change, whereas the edge-exposed MoS_2 shows a characteristic reaction trace (color change). This phenomenon gives evidence for the proposed lateral inward pathway for MoS_2. It is acknowledged that the basal plane of a perfect 2D TMD is impermeable to all atoms and molecules under the ambient condition because of the dense electron cloud.[38] For this reason, the penetration reaction from the basal plane of MoS_2 would not happen. Compared to the basal plane, the edge sites are thought to be electrochemically active. The on-chip experiments have solidly demonstrated the exfoliation process of MoS_2 in the $ZnSO_4$ electrolyte, which inspired us to examine the potential of large-scale production through this strategy. Hence, we transfer bulk MoS_2 samples to the fresh titanium (Ti) foil to carry out the same electrochemical treatment. We monitored the optical video of several dispersive

MoS_2 sheets during the electrochemical process (Video in the Supporting Information). The images of MoS_2 at selected potential are shown in **Figure 4**a, which shows the same inward reaction pathway as proposed. When the anodic potential was higher than ≈1 V, the reaction began from the edge outline and then went straight into the bulk of MoS_2. According to the same results from the bottom contact configuration in this test system and lateral contact in the on-chip device, we demonstrate that the reaction pathway is not decided by the orientation of the electric field but decided by the intrinsic properties of MoS_2. The optical image and Raman spectra of a specific MoS_2 sheet are shown in Figure 4b–d. The Δv between E^1_{2g} and A_{1g} bands of the center region is ≈25.5 cm^{-1}, while Δv of the exfoliated region is 22–23 cm^{-1} (bi/-tri-layer MoS_2). This result also confirms the uniformity of the MoS_2 sample after electrochemical treatment. Meanwhile, we analyze the chemical composition of the MoS_2 sheet after exfoliation. The typical Raman modes of 1T MoS_2 and partially oxidized MoO_x were not detected, demonstrating the maintaining 2H MoS_2 phase (Figure S5, Supporting Information). Similarly, the AFM image further showed the edge regions are involved in the electrochemical reaction, leading to a much-reduced thickness (from 40.9 to 20.7 nm) (Figure S6, Supporting Information). Combined with Raman results, the exfoliated regions are also thought to be stacked by two/three MoS_2 layers. Based on the above results, it is clear that the reaction pathway is lateral inward. Besides, the mass production is also demonstrated as the bottom contact does not affect the proposed reaction pathway and the exfoliated MoS_2 can be easily achieved at a high anodic potential.

To investigate the universality of this electrochemical treatment to other TMD, we further fabricated on-chip $MoSe_2$ devices. Although the CV curves of $MoSe_2$ are similar to those

ADVANCED
SCIENCE NEWS
www.advancedsciencenews.com

ADVANCED
FUNCTIONAL
MATERIALS
www.afm-journal.de

of MoS_2 (shown in Figure S7 in the Supporting Information, oxidation peaks keep increasing during the first several CV cycles), the morphology of $MoSe_2$ after electrochemical treatment shows the different states. From the optical image, two notches along the PMMA window can be found, which potentially indicates that the edge of $MoSe_2$ is completely etched (Figure S8, Supporting Information). Nevertheless, the Raman mapping of the intensity of A_{1g} mode shows the whole outline for $MoSe_2$ after treatment (Figure S8b,e, Supporting Information). Then we analyze the position mapping of the A_{1g} band (Figure S8c,f, Supporting Information), which shows that the invisible part of $MoSe_2$ (notch region) exists as the ultra-thin layer (ν_{A1g} decrease from ≈242 to ≈240 cm^{-1}). Because the weak E^1_{2g} vibration band cannot be observed, the shift of A_{1g} mode is considered to be an index for the layer number less than 5 layers.[37] The redshift of A_{1g} to ≈240 cm^{-1} is attributed to monolayer or bilayer $MoSe_2$. Considering the color and transparency of the $MoSe_2$ edge region, it is rational to suppose that the edge is merely single or a few atomic layers. We further observed the dynamic change of $MoSe_2$ during electrochemical treatment (Figure S9, Supporting Information). Similarly, when anodic potential rises to 1 V versus SCE, an inward reaction began and a transparent trace was lastly left. The further Raman spectra are the same as the results from the on-chip device (Figure S10, Supporting Information), A_{1g} mode of reaction part can still be observed, while ν_{A1g} shifts to ≈240 cm^{-1} (mono/bi-layer $MoSe_2$). The AFM results also confirmed this conclusion, which shows a thickness of ≈2 nm in the exfoliated region (Figure S11,

Supporting Information). To demonstrate the structure of exfoliated $MoSe_2$, cross-sectional HAADF-STEM was used to observe the exfoliated $MoSe_2$. As shown in Figure S12 in the Supporting Information, the STEM images show a gradually reduced thickness of $MoSe_2$. The right side is the bulk phase and the left side is only 1–3 layer. The transition zone (Figure S12c, Supporting Information) shows a continuous reduction of thickness which is different from the sharp shrinking of MoS_2.

To identify the difference between the exfoliated MoS_2 and $MoSe_2$, we analyze the layer-dependent energy band of MoS_2 and $MoSe_2$. The electronic properties of the atomically thin MoS_2 and $MoSe_2$ are dominated by the quantum confinement, which causes an expanded bandgap and transition from indirect to direct gap when thickness decreases to monolayer.[39] **Figure 5**a shows the layer dependent valance band plotted versus vacuum level and standard hydrogen electrode (SHE). The red region represents the redox potential peak of Mo oxidation (0.95–1.15 V vs SHE), according to the CV results. Based on the previous work,[31,40] we thought that the reaction equation is $MoX_2 + 8H_2O \rightarrow Mo^{6+} + 2XO_4^{2-} + 16H^+ + 18e^-$ (X represents S and Se). The valance bands of bulk and monolayer $MoSe_2$ match the redox region, thus the $MoSe_2$ flakes are oxidized. Meanwhile the strong coupling of the bottom layer $MoSe_2$ to the SiO_2 results in a band shift of $MoSe_2$.[12,41] Hence, only the bottom layer $MoSe_2$ is left after the electrochemical oxidation reaction. In another case, we also found a similar phenomenon in a metallic VSe_2, which only left the bottom layers on Ti foil (Figure S13, Supporting Information). Extend this concept to
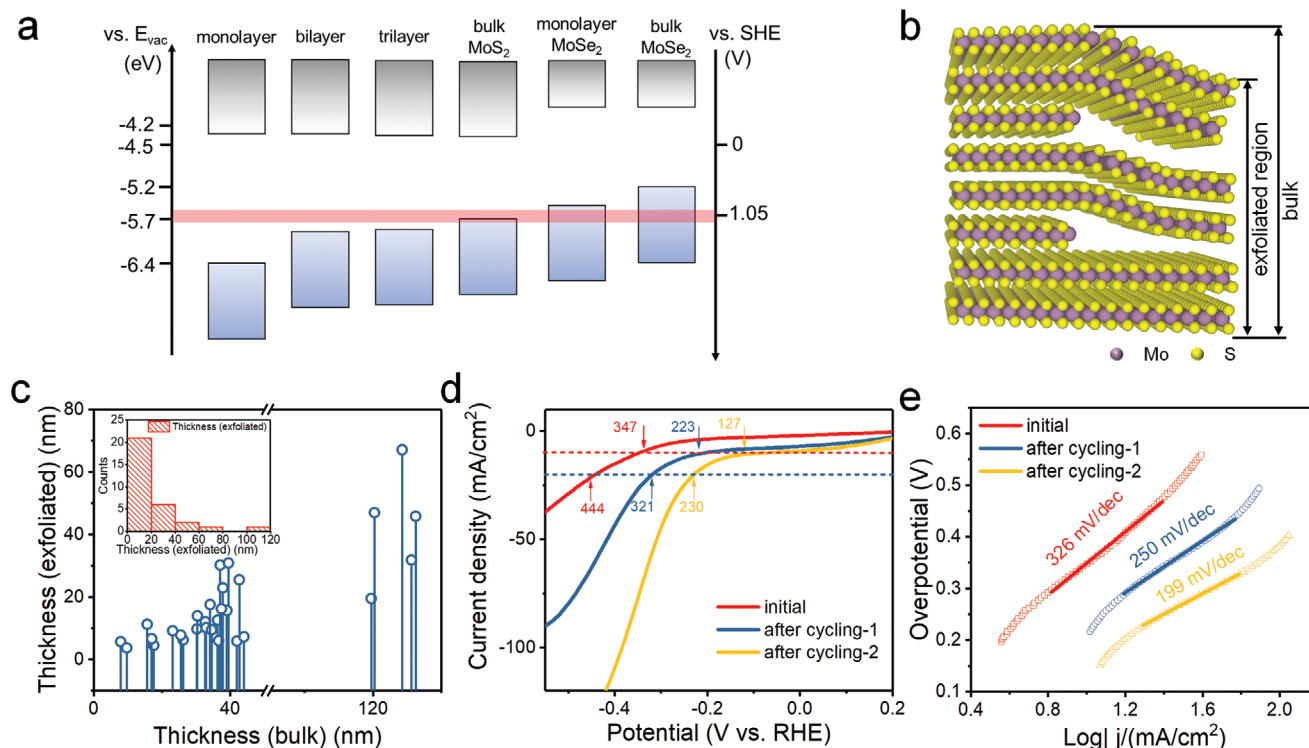

Figure 5. a) Energy band diagrams of MoS_2 and $MoSe_2$ with different layers. The red band represents the redox potential range. The valence band level and bandgap data are adapted from refs. [50] and [51] b) The schematic of the thickness of the edge and the basal plane of MoS_2 after exfoliation. c) The relationship between bulk thickness and exfoliated thickness. Inset: histogram of exfoliated thickness distribution. d) The polarization curves of MoS_2 after different CV cycles treatment (0, 200, and 300 cycles). The dash lines mark the overpotential at 10 and 20 mA cm^{-2}. e) The corresponding Tafel slope plots.

MoS$_2$, the mono-, bi-, and tri-layer MoS$_2$ shows a slight lower valance band than the oxidation region, while the bulk MoS$_2$ valence band falls into the region. Thus, the bulk MoS$_2$ will be electrochemically exfoliated into a series of tri-layer MoS$_2$ flakes. Since the thermal vibration at room temperature is ≈100 meV and the bilayer and trilayer MoS$_2$ valence bands are too close, some bilayer MoS$_2$ can also be found after the electrochemical exfoliation. Based on that analysis, we demonstrated that the specific reaction mechanism of MoS$_2$ is dominated by the layer-dependent electronic properties. In addition to the layer dependent properties, the different edge sites also determine the intrinsic properties. Uncoordinated Mo and S terminal atoms result in two different edge states, zigzag and armchair types.[42] These two edge types result in different electronic properties, show metallic behavior for zigzag and semiconductive for armchair. These characteristics are supposed to account for the selective extraction of some layers due to the coexistence of Mo and S terminal atoms in bulk MoS$_2$. Then we investigate the thickness distribution after 50 CV cycles treatment (Figure 5b,c). Although the correlation between plane thickness and exfoliated thickness remains uncertain, and the thickness of most MoS$_2$ sheets after the reaction is found to be below 20 nm. We then performed the same CV treatment in another electrolyte (Li$_2$SO$_4$ and Na$_2$SO$_4$) (Figures S14 and S15, Supporting Information). The phenomenon is similar for MoS$_2$ in these two electrolytes, while the exfoliated thickness is hard to reach bilayer according to the Raman results.

At last, we explored the application of this original basal plane stacked structure. MoS$_2$ is thought to be a promising candidate for electrocatalytic hydrogen evolution reaction (HER) due to the moderate hydrogen adsorption energy on edge sites.[43] We applied the exfoliated stacked MoS$_2$ as catalyst for HER. The polarization curves of one individual MoS$_2$ sheet after different CV cycles treatment are recorded in 0.5 M H$_2$SO$_4$ based on the on-chip MoS$_2$ device. By electrochemically exfoliating the bulk MoS$_2$ to the stacked bi/tri-layered one, the overpotential decreases from 347 to 127 mV at 10 mA cm^{-2}, and the Tafel slope decreases from 326 to 199 mV dec^{-1} (Figure 5d,e). Considering the charge injection from the electrode, the electrons in bulk MoS$_2$ transport through hopping in the vertical direction. The large Van der Waals gap results in a ≈0.12 eV gap for electron hopping.[44] The reduced thickness of MoS$_2$ reduces the potential gap for electron transfer between layers, thus enhances HER performance. Furthermore, the electronic states of the edge sites on atomically thin MoS$_2$ are more favorable. This performance improvement is attributed to that the expanded edge sites with few atomic layers increases more available active sites and the reduced thickness improves the hydrogen adsorption energy. The much improved HER performance is an example of the application of this stacked MoS$_2$ structure in TMD electrocatalysis.

Besides, atomically thin TMDs have been investigated as the substrate for surface-enhanced Raman spectroscopy (SERS).[45,46] The mechanism for Raman enhancement of TMDs is attributed to the chemical interaction between TMDs and analyte, which is relatively weaker than the electromagnetic field enhancement of noble metal.[47] Hence, an efficient MoS$_2$ SERS substrate without noble metal is eagerly awaited. We further measured the SERS sensitivity of the exfoliated MoS$_2$

using rhodamine 6G (R6G) as the analyte (Figure S16a, Supporting Information). The Raman spectra of R6G on bulk and exfoliated MoS$_2$ are shown in **Figure 6**a,b. We found that the Raman signal of R6G can be detected on the exfoliated MoS$_2$ at an ultra-low concentration of 10^{-8} M (Figure 6b), while the bulk MoS$_2$ only shows a weak signal when the concentration is more than 10^{-3} M. The enhancement factor (EF) can be calculated by,

$$EF = \left(\frac{I_{SERS}}{C_{SERS}}\right) \Big/ \left(\frac{I_N}{C_N}\right),$$ [48] where I$_{SERS}$ and I$_N$ represent the intensity of SERS and normal Raman measurement of R6G, and C$_{SERS}$ and C$_N$ represent the concentration of R6G for SERS and normal Raman measurement, respectively. Hence, the EF of exfoliated MoS$_2$ is 1.15 × 10^5 which is almost three orders of magnitude larger than that of the bulk MoS$_2$ (Figure S16b, Supporting Information). We then recorded the Raman spectra at different regions of an individual MoS$_2$ to demonstrate the enhancement dependence on the state of MoS$_2$ (R6G concentration is 1 × 10^{-5} M). The Raman spectra, optical image, and the max intensity plot are shown in Figure 6c–e. We find that the Ti substrate shows no enhancement of the Raman signal, as well as the bulk MoS$_2$ region shows no characteristic peaks of R6G. Meanwhile, the exfoliated region shows much higher enhancement, demonstrating the enhanced sensitivity of exfoliated MoS$_2$. The stacked structure of stacked atomically thin MoS$_2$ favors the adsorption of R6G molecules and the reduced-thickness adjusted the electronic structures. Moreover, the transition region between the bulk and exfoliated MoS$_2$ and the edge regions show even higher enhancement compared to the plane of exfoliated regions. The structure disorder generates more local dipoles to interact with the dipole of the R6G molecule, which is dominant for the SERS effect. Herein, the improved SERS performance is attributed to the stress and structure disorder-induced rich dipole in the stacked MoS$_2$ (especially in the transition zone).

3. Conclusion

In this work, we demonstrated a systematic investigation of a new strategy by electrochemical oxidation of MoS$_2$ that ends up with a stacked few-layer structure. The process is robust and promising in high-efficient and large-scale production since only an anodic potential is required in the ZnSO$_4$ aqueous solution. Different from the previous etching and corrosion approach, this oxidation is a selective process that leaves uniform bi/tri-layer MoS$_2$ with self-stacked 2D channels. We proved the validity of the electrochemical oxidation-driven exfoliation by on-chip individual MoS$_2$ sheet device and in situ optical observation. Through the comparison between MoSe$_2$ and MoS$_2$, it is found that the relative high valance band causes a different morphology after electrochemical treatment. The strategy is a promising exfoliation method for TMDs, which is ultrafast (tens of second), uniform atomically thin (two/three layers), and high retention (30–40%). The exfoliated few-layer MoS$_2$ is demonstrated to be more efficient as an electrocatalyst for HER which shows a lower overpotential (127 mV) compared to bulk MoS$_2$ (347 mV). Besides, the exfoliated MoS$_2$ is proved to dramatically enhance the sensitivity enhancement factor (1.15 × 10^5) for SERS using

ADVANCED
SCIENCE NEWS

www.advancedsciencenews.com

ADVANCED
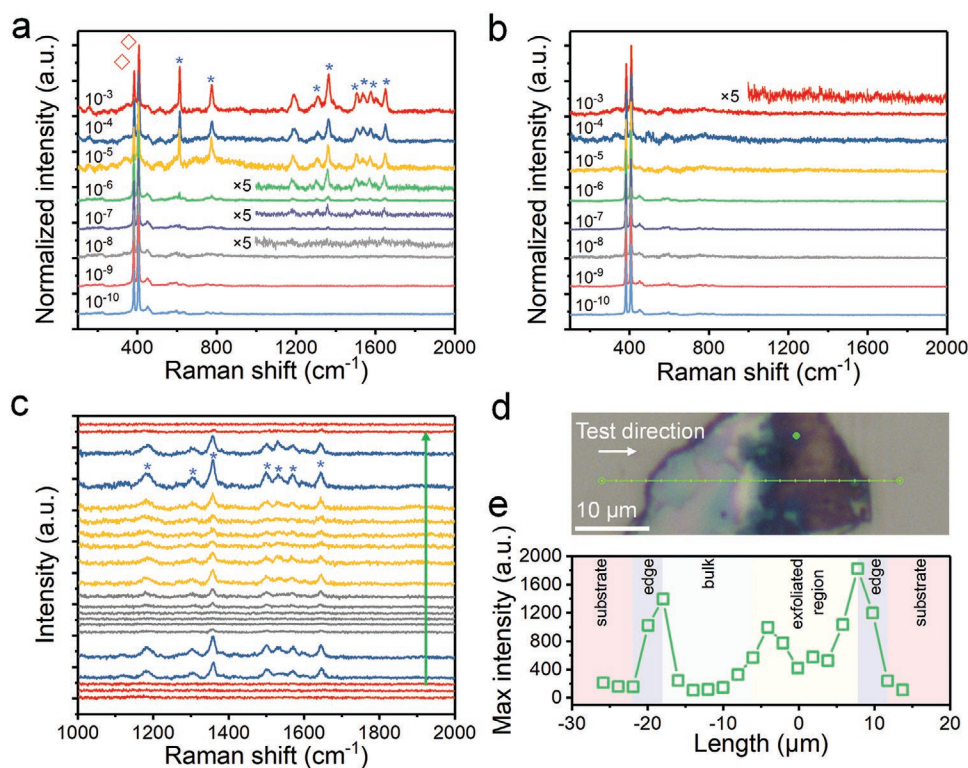**FUNCTIONAL**
MATERIALS

www.afm-journal.de

Figure 6. a) Raman spectra of R6G with different concentration adsorbed on the exfoliated MoS_2. The rhombuses and asterisks denote the characteristic Raman vibration bands of MoS_2 and R6G. The intensity is normalized by the intensity of A_{1g} bands of MoS_2. b) Raman spectra of R6G with different concentration adsorbed on bulk MoS_2. c) Line scan of Raman spectra along the green dot line in figure (d). e) Optical image of a MoS_2 sheet on Ti foil after electrochemical exfoliation with one half-part exfoliated into thin layers. The green dot line represents the Raman mapping test direction in figure (c). d) The maximum intensity of R6G vibration bands along the test line.

10^{-8} M R6G as a target analyte. At last, it is believed that due to the reassembled atomically thin structure, the exfoliated few-layer MoS_2 would have broad application potential in nano-fluid, confined electrocatalysis, quantum devices, and sensor, etc.

4. Experimental Section

Fabrication of the Individual MoS_2 Sheet On-Chip Device: Commercial bulk MoS_2 sheets were transferred by scotch-tape onto the Si/SiO_2 substrate with the patterned gold electrodes. The detailed device fabrication process can be found in the previous work.[8,49] The gold electrodes connected to MoS_2 were fabricated by EBL (JC Nabity Lithography Systems, Nanometer Pattern Generation System) and thermal evaporation deposition (10 nm Ti/150 nm Au, Kurt J. Lesker, PVD75). The PMMA (MicroChem Corp.) windows were opened by EBL to expose the specific regions of the MoS_2 sheet.

Material and Device Characterization: The optical images of the MoS_2 and $MoSe_2$ devices and the in situ observation were taken by optical microscopy (Sunny Optics, 50/100× objective). The Raman spectra were acquired with an excitation laser of 532 nm by Horiba LabRAM HR Evolution. The thickness was measured by AIST-NT SmartSPM 1000 scanning probe microscopy. The cross-sectional sample was prepared by a dual-beam FIB (FEI Helios Nanolab G3) and the STEM images were recorded in a CEOS probe corrected FEI Themis TEM with 300 kV accelerating voltage.

Electrochemical Measurement: A typical electrochemical measurement was performed by a three-electrode configuration based on the on-chip device, where an individual MoS_2 sheet was the working electrode, and platinum wire electrode and saturated calomel electrode (SCE) worked

as the counter and reference electrode. A probe station (Lake Shore, TTPX) was used to connect the working electrode and electrochemical measurement was performed by Autolab PGSTAT302N. For a CV measurement in $ZnSO_4$, the potential was scanned from 0.2 to 1.4 V versus SCE with a scan rate of 20/50 mV s^{-1}. For the measurement on Ti foil, an electrolytic cell was used to perform a normal electrochemical test. The polarization curve of HER (linear sweep voltammetry) was measured at a scan rate of 5 mV s^{-1} with a fine graphite rod as a counter electrode instead of the Pt electrode.

SERS Measurement: The R6G ethanol solution with different concentrations was obtained by the sequential diluting method. In a typical SERS measurement on Ti Foil, 2 μL R6G solution was drop-casted on Ti foil (5 × 5 mm) with MoS_2 samples. The Raman spectra were collected by a 532 nm laser dispersed by 600 gr mm^{-1} gratings (100× objective lens, NA = 0.9), and the power was set as 0.26 mW.

Supporting Information

Supporting Information is available from the Wiley Online Library or from the author.

Conflict of Interest

The authors declare no conflict of interest.

Keywords

[1] S. Manzeli, D. Ovchinnikov, D. Pasquier, O. V. Yazyev, A. Kis, *Nat. Rev. Mater.* **2017**, *2*, 17033.

[2] Q. H. Wang, K. Kalantar-Zadeh, A. Kis, J. N. Coleman, M. S. Strano, *Nat. Nanotechnol.* **2012**, *7*, 699.

[3] B. Radisavljevic, A. Radenovic, J. Brivio, V. Giacometti, A. Kis, *Nat. Nanotechnol.* **2011**, *6*, 147.

[4] Z. Yin, H. Li, H. Li, L. Jiang, Y. Shi, Y. Sun, G. Lu, Q. Zhang, X. Chen, H. Zhang, *ACS Nano* **2012**, *6*, 74.

[5] R. Kumar, N. Goel, M. Kumar, *ACS Sens.* **2017**, *2*, 1744.

[6] L. Li, Z. Qin, L. Ries, S. Hong, T. Michel, J. Yang, C. Salameh, M. Bechelany, P. Miele, D. Kaplan, M. Chhowalla, D. Voiry, *ACS Nano* **2019**, *13*, 6824.

[7] Y. He, Q. He, L. Wang, C. Zhu, P. Golani, A. D. Handoko, X. Yu, C. Gao, M. Ding, X. Wang, *Nat. Mater.* **2019**, *18*, 1098.

[8] J. Wang, M. Yan, K. Zhao, X. Liao, P. Wang, X. Pan, W. Yang, L. Mai, *Adv. Mater.* **2017**, *29*, 1604464.

[9] R. Wang, S. Wang, D. Jin, Y. Zhang, Y. Cai, J. Ma, L. Zhang, *Energy Storage Mater.* **2017**, *9*, 195.

[10] J. Wan, W. Bao, Y. Liu, J. Dai, F. Shen, L. Zhou, X. Cai, D. Urban, Y. Li, K. Jungjohann, M. S. Fuhrer, L. Hu, *Adv. Energy Mater.* **2015**, *5*, 1401742.

[11] A. Kuc, N. Zibouche, T. Heine, *Phys. Rev. B* **2011**, *83*, 245213.

[12] K. F. Mak, C. Lee, J. Hone, J. Shan, T. F. Heinz, *Phys. Rev. Lett.* **2010**, *105*, 136805.

[13] J. N. Coleman, M. Lotya, A. O'Neill, S. D. Bergin, P. J. King, U. Khan, K. Young, A. Gaucher, S. De, R. J. Smith, I. V. Shvets, S. K. Arora, G. Stanton, H. Y. Kim, K. Lee, G. T. Kim, G. S. Duesberg, T. Hallam, J. J. Boland, J. J. Wang, J. F. Donegan, J. C. Grunlan, G. Moriarty, A. Shmeliov, R. J. Nicholls, J. M. Perkins, E. M. Grieveson, K. Theuwissen, D. W. McComb, P. D. Nellist, V. Nicolosi, *Science* **2011**, *331*, 568.

[14] M. Velicky, G. E. Donnelly, W. R. Hendren, S. McFarland, D. Scullion, W. J. I. DeBenedetti, G. C. Correa, Y. Han, A. J. Wain, M. A. Hines, D. A. Muller, K. S. Novoselov, H. D. Abruna, R. M. Bowman, E. J. G. Santos, F. Huang, *ACS Nano* **2018**, *12*, 10463.

[15] Z. Zeng, Z. Yin, X. Huang, H. Li, Q. He, G. Lu, F. Boey, H. Zhang, *Angew. Chem., Int. Ed.* **2011**, *50*, 11093.

[16] S. Tongay, W. Fan, J. Kang, J. Park, U. Koldemir, J. Suh, D. S. Narang, K. Liu, J. Ji, J. Li, *Nano Lett.* **2014**, *14*, 3185.

[17] Z. Cai, B. Liu, X. Zou, H.-M. Cheng, *Chem. Rev.* **2018**, *118*, 6091.

[18] M. Chhowalla, Z. Liu, H. Zhang, *Chem. Soc. Rev.* **2015**, *44*, 2584.

[19] F. Liu, W. Wu, Y. Bai, S. H. Chae, Q. Li, J. Wang, J. Hone, X.-Y. Zhu, *Science* **2020**, *367*, 903.

[20] Y. Chen, L. Gan, H. Li, Y. Ma, T. Zhai, *Adv. Mater.* **2017**, *29*, 1603550.

[21] J. Su, M. Wang, Y. Li, F. Wang, Q. Chen, P. Luo, J. Han, S. Wang, H. Li, T. Zhai, *Adv. Funct. Mater.* **2020**, *30*, 2000240.

[22] A. Zafar, H. Nan, Z. Zafar, Z. Wu, J. Jiang, Y. You, Z. Ni, *Nano Res.* **2017**, *10*, 1608.

[23] M. I. Serna, S. H. Yoo, S. Moreno, Y. Xi, J. P. Oviedo, H. Choi, H. N. Alshareef, M. J. Kim, M. Minary-Jolandan, M. A. Quevedo-Lopez, *ACS Nano* **2016**, *10*, 6054.

[24] Z. Ling, C. E. Ren, M.-Q. Zhao, J. Yang, J. M. Giammarco, J. Qiu, M. W. Barsoum, Y. Gogotsi, *Proc. Natl. Acad. Sci. USA* **2014**, *111*, 16676.

[25] B. Lalmi, H. Oughaddou, H. Enriquez, A. Kara, S. Vizzini, B. Ealet, B. Aufray, *Appl. Phys. Lett.* **2010**, *97*, 223109.

[26] K. K. Kim, A. Hsu, X. Jia, S. M. Kim, Y. Shi, M. Hofmann, D. Nezich, J. F. Rodriguez-Nieva, M. Dresselhaus, T. Palacios, *Nano Lett.* **2012**, *12*, 161.

[27] J.-C. Lei, X. Zhang, Z. Zhou, *Front. Phys.* **2015**, *10*, 276.

[28] X. Wang, S. Kajiyama, H. Iinuma, E. Hosono, S. Oro, I. Moriguchi, M. Okubo, A. Yamada, *Nat. Commun.* **2015**, *6*, 6544.

[29] X. Zhang, Z. Zhang, Z. Zhou, *J. Energy Chem.* **2018**, *27*, 73.

[30] Z. Du, S. Yang, S. Li, J. Lou, S. Zhang, S. Wang, B. Li, Y. Gong, L. Song, X. Zou, *Nature* **2020**, *577*, 492.

[31] S.-S. Wu, T.-X. Huang, K.-Q. Lin, X. Yao, J.-T. Hu, D.-L. Tang, Y.-F. Bao, B. Ren, *2D Mater.* **2019**, *6*, 045052.

[32] H. Li, Q. Yang, F. Mo, G. Liang, Z. Liu, Z. Tang, L. Ma, J. Liu, Z. Shi, C. Zhi, *Energy Storage Mater.* **2019**, *19*, 94.

[33] H. Liang, Z. Cao, F. Ming, W. Zhang, D. H. Anjum, Y. Cui, L. Cavallo, H. N. Alshareef, *Nano Lett.* **2019**, *19*, 3199.

[34] Y. C. Lin, D. O. Dumcenco, Y. S. Huang, K. Suenaga, *Nat. Nanotechnol.* **2014**, *9*, 391.

[35] H. Li, Q. Zhang, C. C. R. Yap, B. K. Tay, T. H. T. Edwin, A. Olivier, D. Baillargeat, *Adv. Funct. Mater.* **2012**, *22*, 1385.

[36] C. Lee, H. Yan, L. E. Brus, T. F. Heinz, J. Hone, S. Ryu, *ACS Nano* **2010**, *4*, 2695.

[37] P. Tonndorf, R. Schmidt, P. Böttger, X. Zhang, J. Börner, A. Liebig, M. Albrecht, C. Kloc, O. Gordan, D. R. Zahn, *Opt. Express* **2013**, *21*, 4908.

[38] S. Hu, M. Lozada-Hidalgo, F. C. Wang, A. Mishchenko, F. Schedin, R. R. Nair, E. W. Hill, D. W. Boukhvalov, M. I. Katsnelson, R. A. Dryfe, I. V. Grigorieva, H. A. Wu, A. K. Geim, *Nature* **2014**, *516*, 227.

[39] A. Splendiani, L. Sun, Y. Zhang, T. Li, J. Kim, C.-Y. Chim, G. Galli, F. Wang, *Nano Lett.* **2010**, *10*, 1271.

[40] K. Sakamaki, K. Hinokuma, A. Fujishima, *J. Vac. Sci. Technol. B* **1991**, *9*, 944.

[41] B. J. Robinson, C. E. Giusca, Y. T. Gonzalez, N. D. Kay, O. Kazakova, O. V. Kolosov, *2D Mater.* **2015**, *2*, 015005.

[42] Y. Li, Z. Zhou, S. Zhang, Z. Chen, *J. Am. Chem. Soc.* **2008**, *130*, 16739.

[43] T. F. Jaramillo, K. P. Jorgensen, J. Bonde, J. H. Nielsen, S. Horch, I. Chorkendorff, *Science* **2007**, *317*, 100.

[44] Y. Yu, S. Y. Huang, Y. Li, S. N. Steinmann, W. Yang, L. Cao, *Nano Lett.* **2014**, *14*, 553.

[45] L. Tao, K. Chen, Z. Chen, C. Cong, C. Qiu, J. Chen, X. Wang, H. Chen, T. Yu, W. Xie, S. Deng, J. B. Xu, *J. Am. Chem. Soc.* **2018**, *140*, 8696.

[46] E. Er, H.-L. Hou, A. Criado, J. Langer, M. Möller, N. Erk, L. M. Liz-Marzán, M. Prato, *Chem. Mater.* **2019**, *31*, 5725.

[47] Y. Yin, P. Miao, Y. Zhang, J. Han, X. Zhang, Y. Gong, L. Gu, C. Xu, T. Yao, P. Xu, Y. Wang, B. Song, S. Jin, *Adv. Funct. Mater.* **2017**, *27*, 1606694.

[48] E. L.e Ru, E. Blackie, M. Meyer, P. G. Etchegoin, *J. Phys. Chem. C* **2007**, *111*, 13794.

[49] M. Y. Yan, X. L. Pan, P. Y. Wang, F. Chen, L. He, G. P. Jiang, J. H. Wang, J. Z. Liu, X. Xu, X. B. Liao, J. H. Yang, L. Q. Mai, *Nano Lett.* **2017**, *17*, 4109.

[50] A. Kumar, P. Ahluwalia, *Eur. Phys. J. B* **2012**, *85*, 186.

[51] J. Padilha, H. Peelaers, A. Janotti, C. Van de Walle, *Phys. Rev. B* **2014**, *90*, 205420.